

Imaging magnetically labeled cells with magnetomotive optical coherence tomography

Amy L. Oldenburg, Jillian R. Gunther, and Stephen A. Boppart

Department of Electrical and Computer Engineering, Beckman Institute for Advanced Science and Technology, University of Illinois at Urbana—Champaign, 405 North Mathews Avenue, Urbana, Illinois 61801

Received November 24, 2004

We introduce a novel contrast mechanism for optical coherence tomography (OCT) whereby the optical scattering of magnetically labeled cells is modified by means of an externally applied magnetic field. This modification is made through the addition of a small electromagnet to the imaging arm of a conventional OCT interferometer. We measure the magnetomotive OCT signal by differencing pairs of axial scans (A-scans) acquired with the magnetic field on and off. Magnetomotive contrast is demonstrated in bulk three-dimensional cell scaffolds containing macrophages labeled with microparticles of iron oxide, demonstrating magnetic-specific contrast over a dynamic range of 30 dB. © 2005 Optical Society of America

OCIS codes: 170.4500, 170.3880, 160.3820, 290.5850.

Optical coherence tomography (OCT) has a unique niche in biomedical imaging by providing cellular-level resolution with a few millimeters of depth penetration at real-time imaging speeds.¹ Increasingly, OCT has played a role in noninvasive *in situ* monitoring of engineered tissue development² within bulk three-dimensional tissue scaffolds. However, the information available through conventional OCT imaging, which senses primarily singly backscattered light, is limited to somewhat nonspecific material properties such as optical scattering, birefringence, and flow properties. Recently there has been interest in developing contrast mechanisms for OCT that are capable of biochemical specificity, i.e., molecular contrast, which would greatly expand the array of biologically relevant information available with OCT.

Efforts toward this goal include interferometric imaging utilizing nonlinear optical effects to detect endogenous molecules through their specific second-harmonic generation signal³ or coherent anti-Stokes Raman scattering profile.⁴ Another attractive approach is the application of exogenous contrast agents with high specificity for the biomolecule of interest *in vivo* or for labeling cells *in vitro*. Protein microspheres incorporating nanoparticles into their shells⁵ and plasmon-resonant gold nanoshells⁶ have been investigated for use as OCT contrast agents because of their high optical scattering efficiencies. Spectroscopic contrast has been demonstrated with near-infrared dyes that exhibit strong wavelength-dependent absorption within the spectral bandwidth of the OCT optical source.⁷ Contrast has also been observed through the optically modifiable absorption properties of Methylene Blue⁸ and Phytochrome A (Ref. 9) dyes in two-color experiments. An advantage to the latter technique is the external modification of a property of the agent, thus permitting background rejection through differencing of pairs of images obtained while the agent's property was changed.

The advantage of difference imaging is exploited here through the interaction between a magnetically susceptible particle (the contrast agent) and an externally applied magnetic field. Magnetomotive contrast is produced by translational force F induced by magnetic field B :

$$\mathbf{F} = \frac{V(\chi_m - \chi_0) \nabla |\mathbf{B}|^2}{2\mu_0}, \quad (1)$$

where V is the particle volume, μ_0 is the permeability constant, and χ_m and χ_0 are the magnetic susceptibilities of the particle and the medium, respectively. Human tissue is only weakly magnetic ($|\chi| \sim 10^{-5}$) compared with biocompatible agents such as iron oxide ($\chi \sim 1$), which has been established as an intravenous magnetic-resonance contrast agent in a clinical setting.¹⁰ The ferromagnetic property of iron oxide also results in an applied torque, $\tau = M \times B$, that is due to remanent magnetization M of the particle. These interactions rotate and translate a magnetic particle within the OCT imaging beam volume as depicted in Fig. 1, resulting in a change in optical scattering that is evident as an amplitude and (or) phase change in the OCT interferogram. In an elastic medium, a restoring force returns the magnetic particle to its original position after the magnetic field is switched off. In this way, modulated application of a magnetic field results in modulation of the OCT signal (Fig. 2). Choice of this modulation frequency outside the bandwidth of the structural OCT signal allows for high background rejection, unlike for passively scattering contrast agents. Here we imple-

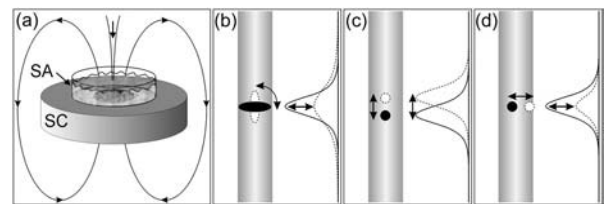


Fig. 1. MMOCT sample configuration. (a) Sample with optical imaging beam and electromagnet (field lines illustrated). SC, solenoid coil; SA, sample. (b)–(d) MMOCT contrast mechanisms illustrating two states of a magnetic microparticle (filled and dash-outlined shapes, respectively) within the imaging focal volume and the associated OCT A-scan demodulated amplitudes (solid and dashed curves, respectively). (b) Rotation of an anisotropic magnetic particle. (c) Axial and (d) transverse displacement of a magnetic particle.

ment magnetomotive OCT (MMOCT) by modulating at half the axial scan frequency such that pairs of A-scans are acquired that correspond to the on and off states of the magnetic field.

The OCT light source consisted of a Ti:sapphire laser (KMLabs, Inc.) centered at 800 nm with a typical bandwidth of 100 nm. This light was launched into a single-mode fiber interferometer that provided 15 mW of optical power at the sample. A galvanometer-mounted retroreflector provided optical delay at 30 Hz, and galvanometer-mounted mirrors provided transverse beam positioning at the sample. The typical imaging resolution with an achromatic imaging lens with 20-mm focal length in the sample arm was $4.5 \mu\text{m}$ axial \times $8 \mu\text{m}$ transverse. A dual-balanced photodetector (New Focus) subtracted the light source noise from the OCT interference signal. Analog and digital bandpass filtering was employed, resulting in a system sensitivity of -101 dB. As shown in Fig. 1(a), a 100-W water-jacketed solenoid coil was placed underneath the sample during imaging. The coil has a 10-mm bore that would also permit beam passage for imaging. The electromagnet's dimensions (outer diameter, 20 mm; thickness, 7 mm) were chosen by use of finite-element calculations to maximize gradient force term $\nabla|B|^2$ from Eq. (1). Teslometer measurements of the magnetic-field strength are consistent with these calculations and suggest $B_{\text{max}}=0.06$ T and $\nabla|B|^2=1.3$ T²/m axially within the OCT imaging volume immediately above the solenoid bore. In the research reported here we use magnetite particles [$\text{Fe}^{(\text{II,III})}_3\text{O}_4$; Sigma Chemical Corp.] average diameter, $1.92 \mu\text{m}$ with a measured $\chi(B_{\text{max}})=3.5$ (superconducting quantum interference device magnetometry). According to Eq. (1), 6.7 pN of force is imparted to a representative magnetite particle with this system.

First we demonstrate the MMOCT principle in a sample of magnetite microparticles embedded in a 5% agarose gel. M-mode images obtained while the power to the electromagnet is modulated (Fig. 2) illustrate the large OCT amplitude modulation (20%

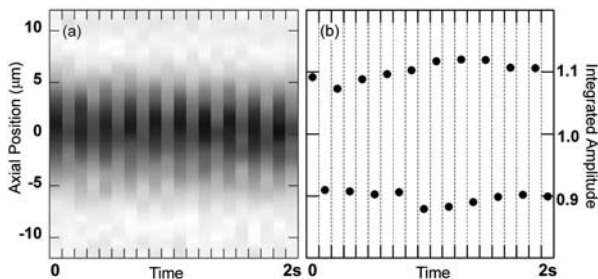


Fig. 2. M-mode OCT imaging. (a) Repetitive axial scans at 10 Hz of a magnetite microparticle embedded within 5% agarose gel during magnetic-field modulation. Each axial scan was acquired with the magnetic field alternately on and off. (b) Integrated demodulated OCT signal amplitude for each axial scan in (a). Magnetically induced displacement of the magnetic particle and subsequent restoration by the agarose medium account for the observed regularity in the modulation of the optical scattering.

in this instance) obtained as a result of magnetomotion. A transverse displacement of $>0.7 \mu\text{m}$ within the imaging beam [Fig. 1(c)] would be sufficient to explain the observed modulation.

For the purposes of discriminating magnetically labeled from unlabeled cells, we define MMOCT signal S at position \mathbf{r} as the ratio of the difference squared obtained during magnetic-field modulation to the expected value of the difference squared in the absence of the magnetic field:

$$S(\mathbf{r}) = \frac{[\alpha_{\text{on}}(\mathbf{r}, t) - \alpha_{\text{off}}(\mathbf{r}, t + \Delta t)]^2}{[\alpha_{\text{off}}(\mathbf{r}, t) - \alpha_{\text{off}}(\mathbf{r}, t + \Delta t)]^2} = \frac{\Delta\alpha_{\text{mod}}^2(\mathbf{r}, \Delta t)}{D_{\alpha_{\text{off}}}(\mathbf{r}, \Delta t)}, \quad (2)$$

where α_{on} and α_{off} are the demodulated (structural) OCT signal amplitudes obtained with the magnetic field on and off, respectively. S is therefore a measurement of the signal-to-noise ratio of the total (magnetic+nonmagnetic) signal to the nonmagnetic noise. Here the elapsed time Δt between successive measurements is the axial scan period. The denominator $D_{\alpha_{\text{off}}}$ is the structure function¹¹ of the random process α_{off} determined by Brownian and cellular motion (speckle noise) and by shot noise, which randomize the measurement of α over time interval Δt . This loss of correlation gives rise to a magnitude dependence in the structure function that is used to eliminate ghosting in the MMOCT image. We estimate $D_{\alpha_{\text{off}}}$ by obtaining an image without magnetic-field modulation [i.e., pairs of $\alpha_{\text{off}}(t)$ and $\alpha_{\text{off}}(t + \Delta t)$] immediately before acquisition of the MMOCT image. We use these background data to determine the magnitude dependence of $D_{\alpha_{\text{off}}}=D_{\alpha_{\text{off}}}(\alpha_{\text{off}}^2)$ by least-squares fitting, which we subsequently use to evaluate MMOCT signal S .

To demonstrate the experimental merit of these concepts, we imaged three-dimensional tissue scaffolds containing subpopulations of magnetically labeled and unlabeled cells. Macrophage cells (J774A.1) were exposed to 1.2 mg/mL of magnetic microparticles (described above) 1 day after subculturing, where they were allowed to uptake the particles by phagocytosis overnight. Macrophage viability after overnight magnetite particle exposure ($>99\%$ after 24 h) was evaluated by Trypan Blue exclusion, and counting indicated no significant difference ($<1\%$) in proliferation of magnetite-exposed macrophages to controls immediately before scaffold preparation. Long-term cell viability in these cell-seeded scaffolds, however, was not investigated in this study. After rinsing of loose cells and particles, cells were embedded in a scaffold consisting of 1% low gel temperature agar, 19% phosphate-buffered saline, and 80% complete growth medium. Control cells were handled identically, except for omission of magnetic particles. Structural OCT and MMOCT images of these cell scaffolds were obtained in tandem (see, e.g., Fig. 3). We acquired background images with which to estimate the structure function specific to each sample. As shown, a large percentage of scatterers in the magnetite-exposed cell scaffold exhibited a magnetic-specific signal. Light microscopy

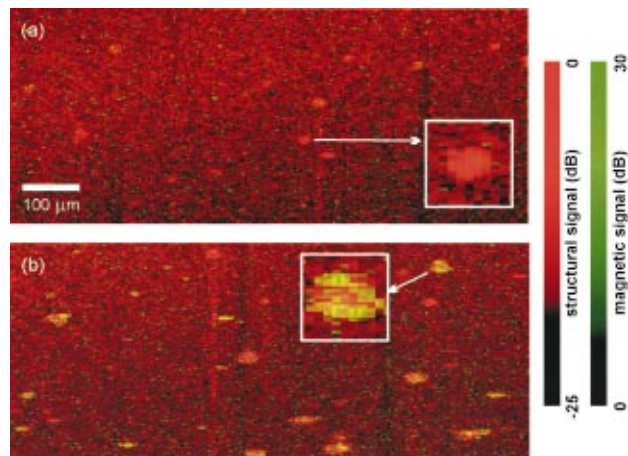


Fig. 3. Representative images of macrophage cells in three-dimensional scaffolds that display structural OCT (red) and MMOCT (green) signals. (a) Control macrophages and (b) macrophages allowed to uptake magnetite microparticles. Insets, $40\ \mu\text{m} \times 40\ \mu\text{m}$. The structural OCT signal is defined as the demodulated interferogram amplitude such that 0 dB is the maximum value. The MMOCT signal is $10 \log(S)$, where S is defined in Eq. (2). Apparent cell sizes (approximately $8\text{--}30\ \mu\text{m}$) are consistent with light microscopy observations.

cell counts indicated three populations of scatterers: unlabeled cells ($38\% \pm 5\%$), magnetically labeled cells ($52\% \pm 6\%$), and loose magnetic particles ($10\% \pm 3\%$), for a total of $62\% \pm 7\%$ magnetically modulated species. This result is consistent with visual analysis of the MMOCT images in which $68\% \pm 8\%$ of the scatterers within the magnetically labeled cell scaffold were identified as magnetic. By comparison, $\leq 1\%$ of the scatterers within the control cell scaffold and within the background image of either scaffold were identified as magnetic.

Mean signal S averaged over the entire image was $0.6\text{--}0.8\ \text{dB}$ for both background images and for the control cell scaffold MMOCT image. In the magnetic cell scaffold MMOCT image the mean signal was $1.5\ \text{dB}$. Magnetic specificity is further emphasized by considering only pixel values above a 10% threshold, over which the mean signal is $11.4\ \text{dB}$ in the magnetic cell scaffold MMOCT image and less than $1\ \text{dB}$ in the background and control scaffold images. The dynamic range ($\sim 30\ \text{dB}$) is limited here by speckle correlation time τ_{corr} , which determines $D_{\text{aoff}}(\Delta t)$ and which is specific to the sample. This range can be improved in either of two ways: reducing Δt to effectively freeze the Brownian and cellular motion or increasing the number of samples of the signal $\Delta\alpha_{\text{mod}}(\Delta t)$ to average over these statistical deviations. The former method yields the minimum value $D_{\text{aoff}}(\Delta t \ll \tau_{\text{corr}}) = 2\sigma_{\text{shot}}^2$ (twice the shot-noise variance). The magnitude of the signal, $\Delta\alpha_{\text{mod}}$, should increase with $\nabla|B|^2$, V , χ_m , and particle density and should decrease with sample elasticity. The average $\Delta\alpha_{\text{mod}}$ for pixels above a 10% threshold was 6% and 35% of α_{off} within the control and the magnetic cell

scaffolds, respectively.

We have demonstrated magnetic-specific contrast with OCT by applying a safe concentration of iron oxide microparticles to macrophage cells. Magnetic particles are desirable because of their ability to externally modulate their scattering outside the bandwidth of the structural OCT signal, eliminating the need for *a priori* structural information to identify the agents. The observed dynamic range of 30 dB may be improved by faster scanning to reduce speckle noise by use of systems such as Fourier-domain OCT,¹² which may also provide improved phase stability for sensing magnetomotive contrast through phase modulation of the OCT signal. The large modulation amplitudes observed (35%) suggest that particle size and concentration do not severely limit this system. In principle, MMOCT can detect nanoscale contrast agents that do not exhibit significant optical scattering but rather act to displace adjacent scatterers such as cells and organelles.

The ability to track labeled cells in millimeter-scale highly scattering tissue volumes provides a new tool for many fields including tissue engineering, developmental biology, and tumor biology. Given the current development of appropriately targeted magnetic particles, the unique scale and speed of MMOCT imaging may also provide a new investigational tool with which to study *in vivo* transport and for molecular contrast imaging.

S. A. Boppart's e-mail address is boppart@uiuc.edu.

References

1. D. Huang, E. A. Swanson, C. P. Lin, J. S. Schuman, W. G. Stinson, W. Chang, M. R. Hee, T. Flotte, K. Gregory, C. A. Puliafito, and J. G. Fujimoto, *Science* **254**, 1178 (1991).
2. W. Tan, A. Sendemir-Urkamaz, L. J. Fahrner, R. Jamison, D. Leckband, and S. A. Boppart, *Tissue Eng.* **10**, 1747 (2004).
3. Y. Jiang, I. Tornov, Y. Wang, and Z. Chen, *Opt. Lett.* **29**, 1090 (2004).
4. D. L. Marks and S. A. Boppart, *Phys. Rev. Lett.* **92**, 123905 (2004).
5. T.-M. Lee, A. L. Oldenburg, S. Sitafalwalla, D. L. Marks, W. Luo, F. Jean-Jacques Toublan, K. S. Suslick, and S. A. Boppart, *Opt. Lett.* **28**, 1546 (2003).
6. C. Loo, A. Lin, L. Hirsch, M.-H. Lee, J. Barton, N. Halas, J. West, and R. Drezek, *Technol. Cancer Res. Treat.* **3**, 33 (2004).
7. C. Xu, J. Ye, D. L. Marks, and S. A. Boppart, *Opt. Lett.* **29**, 1647 (2004).
8. K. D. Rao, M. A. Choma, S. Yazdanfar, A. M. Rollins, and J. A. Izatt, *Opt. Lett.* **28**, 340 (2003).
9. C. Yang, M. A. Choma, L. E. Lamb, J. D. Simon, and J. A. Izatt, *Opt. Lett.* **29**, 1396 (2004).
10. M. G. Harisinghani, J. Barentsz, P. F. Hahn, W. M. Deserno, S. Tabatabaei, C. Hulsbergen van de Kaa, J. de la Rosette, and R. Weissleder, *N. Engl. J. Med.* **348**, 2491 (2003).
11. J. W. Goodman, *Statistical Optics* (Wiley, New York, 1985), pp. 73–79.
12. R. Leitgeb, C. K. Hitzenberger, and A. F. Fercher, *Opt. Express* **11**, 889 (2003), <http://www.opticsexpress.org>.